C.E.D. Riboldi
Energy-Optimal Off-Design Power Management for Hybrid-Electric Aircraft
Aerospace Science and Technology, Vol. 95, 2019, 105507 (16 pages)
doi:10.1016/j.ast.2019.105507

Energy-Optimal Off-Design Power Management for Hybrid-Electric Aircraft

Carlo E.D. Riboldi*

[a]*Department of Aerospace Science and Technology, Politecnico di Milano, Milano, Via La Masa 34, 20156 Italy*

Abstract

Among the advantages associated with the adoption of hybrid-electric power-trains in aviation is the greater flexibility that this type of propulsion system offers. This results in the ability to fly an assigned mission profile making suitable use of both the electric and fuel-burning power components, based on a power management strategy targeting diverse alternative specific needs, like for instance reduced energy consumption or lower noise emission. However, the greater flexibility of a hybrid-electric power-train comes together with an increased complexity in its design and operation. Integrated design procedures for hybrid-electric aircraft have been the target of previous works, whereas the present paper focuses on the quantification of the off-design characteristics of an already defined hybrid-electric design. To this aim, the power management strategy is considered as configurable. The problem of how to balance electric and mechanical power, accounting for the limited energy availability on board while coping with generic mission requirements, is investigated. In order to smartly obtain the desired strategy, the paper introduces an optimal approach, capable of reducing energy expenditure by properly setting the throttle of the fuel-burning and electric components, in coordination with the amount of battery recharging power. The method is explained with a rigorous mathematical approach, and thoroughly tested on a realistic test-bed.

Keywords:

hybrid-electric aircraft, power management strategy, off-design testing, optimal approach

Nomenclature

$\boldsymbol{S}$	Set of optimization constraints
$\boldsymbol{q}$	Array of optimization parameters
C_D	Drag coefficient
C_L	Lift coefficient
$C_{\mathrm{L,max}}^{\mathrm{clean}}$	Maximum lift coefficient in clean configuration
$C_{D,0}^{\mathrm{clean}}$	Parasite drag coefficient (parabolic polar), clean configuration

*Corresponding author, *Tel.:* +39-02-2399-8609; *Fax:* +39-02-2399-8334.
Email address: carlo.riboldi@polimi.it (Carlo E.D. Riboldi)

$E_{\text{bat,max}}$	Energy stored in battery, maximum by design
E_{bat}	Current energy stored in battery
$E_{\text{fuel,max}}$	Energy stored in fuel, maximum by design
E_{fuel}	Current energy stored in fuel
H	Total altitude
J	Cost function for optimization
K^{clean}	Induced drag parameter (parabolic polar), clean configuration
L	Design take-off length
P_{a}	Power available
$P_{\text{EM,n}}$	Nominal power of the EM
$P_{\text{ICE,n}}$	Nominal power of the ICE
P_{rec}	Battery recharge power
P_{r}	Power required for horizontal flight
R	Range
R_{t}	Range target
S	Reference wing surface
S_{i}	i-th component of the set of optimization constraints
T	Time of flight
V	Airspeed
V_{stall}	Stall speed
W	Current aircraft weight
W_{bat}	Battery weight
$W_{\text{fuel,max}}$	Fuel weight, maximum by design
W_{fuel}	Current fuel weight

W_{to}	Take-off weight, maximum by design
EM	Electric motor
ICE	Internal combustion engine
e_{bat}	Energy mass-density for battery
e_{fuel}	Energy mass-density for fuel
g	Gravitational acceleration
h	Altitude
h_{e}	Energy altitude of all energy storage systems
h_{bat}	Battery energy altitude
h_{fuel}	Fuel energy altitude
h_{t}	Altitude target
p_{bat}	Power mass-density for battery
t_0	Initial time
t_{f}	Final time
η_{disc}	Efficiency of the battery discharging process
η_{gen}	Efficiency of the electric generator
$\eta_{\text{ICE,n}}$	Efficiency of the ICE, nominal
η_{ICE}	Current efficiency of the ICE
η_{P}	Propeller gearbox and propulsive efficiency
η_{rec}	Efficiency of the battery recharging process
ρ	Density of air
σ_{EM}	Throttle setting, EM
σ_{ICE}	Throttle setting, ICE
τ_{rec}	Ratio of battery recharge over available mechanical power

$\zeta_{\text{bat,final}}$	Ratio of initial battery energy over maximum by design, final value
$\zeta_{\text{bat,min}}$	Ratio of initial battery energy over maximum by design, minimum value
ζ_{bat}	Ratio of initial battery energy over maximum by design
ζ_{fuel}	Ratio of initial fuel energy over maximum by design
$(\cdot)^{\text{climb}}$	Related to climb phase
$(\cdot)^{\text{cruise}}$	Related to cruise phase
$(\cdot)^{\text{descent}}$	Related to descent phase
$(\cdot)^{\text{loiter}}$	Related to loiter phase
$(\cdot)^{\text{take-off}}$	Related to take-off phase
$\dot{(\cdot)}$	Time derivative

1. Introduction

Hybrid-electric power-trains for aviation are gaining more and more interest in research and industry, for they feature a greater flexibility compared to more widespread propulsive solutions, and are henceforth capable of meeting diverse design needs. In particular, while not renouncing to high power-to-weight and energy-to-weight ratios necessary for good flight performance, and more typical to conventional (i.e. fuel-burning) propulsion, the presence of an electric component in a hybrid-electric power-train allows to mitigate the noise and pollutant emissions for part of the mission with respect to a conventionally propelled aircraft. This greatly increases comfort on board and acceptance by local communities [1, 2, 3, 4, 5], both crucial aspects especially in the field of lighter aviation operating from smaller airfields, which in turn are being currently reconsidered for commercial operations [6], showing a potentially dramatic impact of hybrid-electric aviation at a system level [7].

However, the greater flexibility of hybrid-electric power-trains is associated to an increase in the complexity of the design process, starting from the preliminary sizing stage. Due to the coexistence of fuel-based and electricity-based systems and their respective storage, conversion and distribution sub-systems, the number of components is higher with respect to conventional power-trains. This means a significant increase in the propulsion-related shares of the take-off weight to be sized in the initial phases of the design. The inherent features of the electric part make classical sizing method based on fuel fractions inapplicable [8]. The hybrid-electric aircraft sizing problem, featuring a space of solutions with more dimensions than for conventional

aircraft, is often treated with customized design procedures [4, 9, 10], which, albeit satisfactory to treat a particular design case, do not offer any guarantee of optimality neither in terms of energy and power installed, nor of weight - i.e. the resulting aircraft might be heavier, load more energy or power than needed for an intended target mission profile. To cope with the increased complexity of the preliminary sizing in a more holistic way, design procedures have been proposed [11, 12] that adopt a weight-optimal approach, retrieved from design techniques typical to conventionally-propelled aircraft, and declined to the case of a hybrid-electric power-train. In these methods, an automatic optimization process is envisaged, seeking for an optimum in terms of lowest energy expenditure, weight and cost, mathematically closing the preliminary sizing problem with constraints coming from the mission profile and from a certification framework, considered mostly relevant for a specific aircraft category. One of these techniques [12] faces the coupling of installed power and energy, and their respective power settings over the mission, simultaneously returning an optimal sizing of the power-train and an optimal power management strategy for covering an assigned design mission.

While the techniques just cited allow to end up with an optimal design solution coping with the requirements of a specific mission, the performance of the new aircraft in off-design conditions, i.e. when the mission profile, or the initial energy of fuel and batteries are not as assumed at the design level, has not been studied thoroughly. Such analysis is especially relevant for exploiting the potential of hybrid-electric power-trains, which differently from standard ICE or electric propulsion systems, offer more degrees of freedom in energy management, through the coordinated use of energy sources on-board, represented by fuel and batteries. This feature, specific to hybrid-electric aircraft, typically allows to pursue a strategy to maximize some selected energy-related flight performance coping with diverse mission initial and boundary conditions, while simultaneously keeping compliant with all design requirements. The off-design problem has been treated in the past in the field of hybrid-electric land vehicles, showing the relevance of a comprehensive approach yielding an automatized solution to the problem of power settings for a planned trajectory, in order to exploit the flexibility of a hybrid-electric power-train for optimizing some specific performance index [13, 14]. For aircraft, some solutions have been introduced with success, coping with specific cases and limitations of existing measurement systems [15].

The present paper investigates the off-design performance issues for hybrid-electric aircraft, facing the problem in a general way as a new design problem, where differently from the preliminary sizing phase most of the aircraft weights are known, but the power settings of the energy conversion systems and the battery recharge power are treated as free variables, set to meet the requirements of a new, off-design mission. The methodology is presented for the case of a single-engine propeller-driven aircraft, hence finding direct application in the lower-weight general aviation field, but it is designed to be extendable to more complex propulsion configurations without relevant theoretical implications. As a product of the proposed procedure, the power settings and battery recharge power are found as piece-wise constant functions of time, solving an

energy-optimal problem. This way, the present work not only extends the analysis of the design problem for hybrid-electric aircraft, presented in previous works [11, 12], but it investigates a novel general methodology to bear an optimal power management strategy, coping with very generic starting conditions and mission requirements, smartly exploiting the flexibility of the hybrid-electric power-train.

In a first part, the paper will recall the analytic models adopted for the power-train, based on energy and power balance equations, sufficiently general to be applicable to both a pure-series, pure-parallel or an intermediate series-parallel case [16]. The energy-optimal problem will be analyzed next, with a focus on the series-parallel case, which offers the greatest flexibility and makes the energy-optimal design problem more articulated. Finally, the performance in off-design conditions obtained following an energy-optimal management of the power settings is quantitatively analyzed considering the case of an example hybrid-electric motor-glider. To improve the readability of results, the off-design analysis will be carried out considering a basic mission, consisting of climb, cruise and descent. This is not a simplistic assumption though, as most aircraft especially in the sport category usually fly cross-country missions structured on just these segments. Furthermore, it will be shown how the peculiarities of such legs of the mission need to be accounted for with care, in order to pose the power management problem in a mathematically sound way.

2. Mathematical model of a hybrid-electric aircraft

This section presents at first the key relationships featured in the model of a hybrid-electric power-train considered here, and secondarily how they can be used to match the typical mathematical model of an aircraft in flight.

2.1. Modeling a hybrid-electric power-train

The functional scheme of a generic hybrid-electric power-train is presented in Fig. 1. Considered energy storage systems are both the fuel tank, associated to a maximum fuel weight $W_{\mathrm{fuel,max}}$, and the battery, associated to a battery weight W_{bat}.

The energy quotas pertaining to these sub-systems can be obtained from the respective energy densities, e_{fuel} and e_{bat}, such that the maximum energy which can be stored in the fuel is $E_{\mathrm{fuel,max}} = \frac{W_{\mathrm{fuel,max}}}{g e_{\mathrm{fuel}}}$, whereas the top energy in the battery is $E_{\mathrm{bat,max}} = \frac{W_{\mathrm{bat}}}{g e_{\mathrm{bat}}}$, where g is gravity.

The scheme in Fig. 1 features two conversion systems, namely an internal combustion engine (ICE) and an electric motor (EM). The first operates converting the chemical power associated to a fuel flow $\dot{W}_{\mathrm{fuel}}$ into mechanical power, which from a functional viewpoint can be split in two components. One is input directly to the gearbox and to the propeller, whereas the other is a recharge power component, used to recharge the batteries. This latter component is fed to a generator, producing an electric power flow recharging the

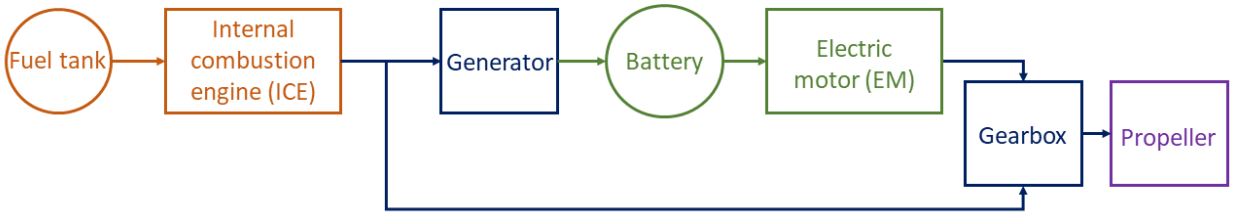

Figure 1: Schematic functional representation of a generic hybrid-electric power-train. Amber: fuel storage and conversion. Green: electric energy storage and conversion. Dark blue: mechanical power conversion and routing. Purple: mechanical to aerodynamic propulsion conversion.

battery. On the other hand, the battery is drained by the electrical motor, which produces mechanical power fed to the gearbox and to the propeller.

It can be observed that this model is directly applicable to a single-ICE, single-EM case, which as noted will be treated here for simplicity. However, no more functional areas should be present on multi-ICE/EM aircraft, typically placed in heavier weight categories, but only a larger number of components of the same types considered here. Apart from an obvious increase in complexity in the setup of the models and management methods presented next, no significant conceptual difference is expected, making the simpler theoretical example presented here meaningful and interesting in itself.

Considering Fig. 1, the power output of the propeller can be written as follows

$$P_{\mathrm{a}} = \left(\sigma_{\mathrm{ICE}} P_{\mathrm{ICE,n}} - P_{\mathrm{rec}} + \sigma_{\mathrm{EM}} P_{\mathrm{EM,n}}\right) \eta_{\mathrm{P}}. \tag{1}$$

Here σ_{ICE} and σ_{EM} are the thrust settings, varying between 0 and 1, whereas $P_{\mathrm{ICE,n}}$ and $P_{\mathrm{EM,n}}$ are the nominal installed power of the ICE and EM respectively. Recharge power P_{rec} represents the component of the ICE output destined to recharge the battery. Finally, η_{P} is the efficiency of the propeller and gearbox, typically depending on current flight conditions.

It is noteworthy that the extreme cases of a pure-series and a pure-parallel hybrid-electric power-train behavior can be modeled by setting a suitable value of P_{rec}. In particular, for a pure-series all ICE power is used to recharge the batteries, yielding the equivalence $P_{\mathrm{rec}} = \sigma_{\mathrm{ICE}} P_{\mathrm{ICE,n}} \eta_{\mathrm{ICE}}$, and consequently the available power is $P_{\mathrm{a}} = \sigma_{\mathrm{EM}} P_{\mathrm{EM,n}} \eta_{\mathrm{EM}} \eta_{\mathrm{P}}$ in this case. Conversely, for a pure-parallel $P_{\mathrm{rec}} = 0$, and as a consequence $P_{\mathrm{a}} = \left(\sigma_{\mathrm{ICE}} P_{\mathrm{ICE,n}} \eta_{\mathrm{ICE}} + \sigma_{\mathrm{EM}} P_{\mathrm{EM,n}} \eta_{\mathrm{EM}}\right) \eta_{\mathrm{P}}$, showing that all power from the ICE and EM is conveyed to the propeller in this case.

Further balance equations related to the scheme in Fig. 1 can be written for the storage systems. For the

fuel tank, the fuel flow should match the power output by the ICE, yielding

$$\dot{W}_{\text{fuel}} = \frac{\sigma_{\text{ICE}} P_{\text{ICE,n}} g}{e_{\text{fuel}} \eta_{\text{ICE}}}, \tag{2}$$

where η_{ICE} is the conversion efficiency of the ICE, typically a function of (at least) the throttle parameter σ_{ICE}. The weight balance Eq. 2 can be rewritten as a power balance equation by taking e_{fuel} to the left hand side, and by defining the energy associated to the on-board fuel as $E_{\text{fuel}} = \frac{W_{\text{fuel}} e_{\text{fuel}}}{g}$.

Defining the energy currently stored in the battery as E_{bat}, it is possible to write the power balance equation for the battery as

$$\dot{E}_{\text{bat}} = P_{\text{rec}} \eta_{\text{gen}} \eta_{\text{rec}} - \frac{\sigma_{\text{EM}} P_{\text{EM,n}}}{\eta_{\text{EM}} \eta_{\text{disc}}} \tag{3}$$

where η_{gen} is the efficiency of the generator, η_{rec} that of the battery recharging process, η_{disc} the efficiency of the battery discharging process, and η_{EM} that of the electric motor.

2.2. Energy-based model of a flight mission

In order to explore the limits of the performance of a newly designed aircraft at a preliminary stage, a simplified point-mass model can be adopted to describe the physics of an assigned mission profile.

Under the hypothesis of calm air (i.e. no wind), a power balance equation capable of describing both horizontal and climb/descent phases, also in presence of acceleration along the point-mass trajectory, i.e. the direction of the airspeed vector, can be obtained multiplying the force equilibrium equation written in the direction normal to the airspeed vector by the value of the airspeed V. This process produces the following expression

$$\frac{P_{\text{a}} - P_{\text{r}}}{W} = \dot{H}, \tag{4}$$

where P_{a} is power available, defined in Eq. 1, P_{r} is power required for horizontal flight, W is the current weight of the aircraft and H is total altitude. Power required P_{r} represents the power needed for equilibrium in horizontal flight at airspeed V, at an altitude h represented by density $\rho(h)$, for an aircraft with reference wing surface S, weight W, developing a drag coefficient $C_D = C_D(C_L) = C_D\left(\frac{W}{\frac{1}{2}\rho V^2 S}\right)$, as

$$P_{\text{r}} = \frac{1}{2}\rho V^3 S C_D. \tag{5}$$

The variable total altitude is defined as [17]

$$H = h + \frac{V^2}{2g}, \tag{6}$$

and is such that its time derivative is

$$\dot{H} = \dot{h} + \frac{\dot{V} V}{g}, \tag{7}$$

appearing on the right-hand side of Eq. 4, where h is altitude, and $\dot{h}$ represents vertical speed.

The power balance equation (Eq. 4) can be adopted to describe level flight, climb and descent, which can be assembled to create a generic flight profile representative of a standard mission of most cross-country flights in the general aviation field, as well as in commercial operations.

In particular, considering a flight phase operated at constant altitude, it can be assumed that $\dot{h} = 0$, yielding a simplification in Eq. 4 such that

$$\frac{P_\mathrm{a} - P_\mathrm{r}}{W} = \frac{\dot{V}V}{g}. \tag{8}$$

For climb and descent both components of $\dot{H}$ in Eq. 7 may be non-null, and their respective values may assume both positive and negative values. This is true also for their sum, which will be typically positive in climb and negative in descent, reflecting the sign of the specific excess power on the left-hand side of Eq. 4.

3. Energy-optimal off-design power management technique

3.1. Introducing off-design performance

In this paper we focus on a specific off-design problem, where the energy levels associated to the fuel and to the battery at the beginning of the flight are different from the design values. This scenario is of great relevance in standard practice, as it is well known especially to pilots and operators of smaller general aviation aircraft. This is due to the lack of services in the majority of the remote destination airports often visited by aircraft in this category, which today - and likely also in the next years as well - hampers the refill of fuel tanks and the recharging of batteries before starting a return flight.

The steps adopted to set up the analysis of this off-design problem will be described in this and the following subsections. Consider a design mission where a minimum target distance R_t has to be covered, and the cruise needs to be operated at a certain altitude h_t. The latter may be due either to air traffic control constraints or for passing over natural obstacles. The take-off condition of the aircraft is characterized by assigned values for the ratios

$$\begin{aligned} \zeta_\mathrm{fuel} &= \frac{E_\mathrm{fuel}\left(t_0\right)}{E_\mathrm{fuel,\,max}} = \frac{W_\mathrm{fuel}\left(t_0\right)}{W_\mathrm{fuel,\,max}} \\ \zeta_\mathrm{bat} &= \frac{E_\mathrm{bat}\left(t_0\right)}{E_\mathrm{bat,\,max}} \end{aligned} \tag{9}$$

where t_0 identifies the starting time of the mission. From the first of the two expressions in Eq. 9, it is clear that the energy associated to the fuel corresponds to a certain amount of fuel weight.

Both ζ_fuel and ζ_bat would be equal to 1 in design conditions, whereas they will be set to values lower than 1 in the considered off-design scenarios. It can be observed that if R_t and h_t are less stringent than in the design case, then $\zeta_\mathrm{fuel} = 1$ and $\zeta_\mathrm{bat} = 1$ - i.e. the design values - would assure meeting such requirements. On the other hand, this is not generally assured for ζ_fuel and ζ_bat lower than 1, unless the requirements expressed by R_t and h_t are consistently reduced.

3.2. Energy-optimal approach

In the scenario introduced in section 3.1, provided the mission targets R_t and h_t are compatible with the values of ζ_fuel and ζ_bat, it is typically possible to complete the mission following several different energy strategies.

To explain this point better, consider Eq. 1, where it is apparent that the power available is a function of three components. At a design level, all variables in that expression, including $P_\mathrm{ICE,n}$ and $P_\mathrm{EM,n}$ can be considered as parameters to be tuned, in order to meet an assigned target performance [12]. On the other hand, as far as an off-design analysis is of interest, such aircraft characteristics - installed power, but also structural mass, battery mass, maximum fuel weight - should be considered as known, whereas the power settings σ_ICE, σ_EM and P_rec can be negotiated to cope with a contingent scenario. These quantities are in principle functions of time over the duration of the mission.

Further quantities that can be tuned are pertinent to the mission profile. In particular, the value of the flight speed V at every time instant during the flight constitutes a free parameter.

Now, a possible way to select a setting for the throttles and speed over the mission profile is that of looking for an energy optimum. A measure of optimality may be assumed as the quantity of energy depleted during the flight, compared to the quantity put on-board at the time of departure. For easing comparisons of the energy levels as described by the total altitude variable H (Eq. 6), it is possible to define the altitudes corresponding to the fuel and battery energy levels at every time during the mission, as

$$\begin{aligned} h_\mathrm{fuel} &= \frac{E_\mathrm{fuel}}{W_\mathrm{take\text{-}off}} \\ h_\mathrm{bat} &= \frac{E_\mathrm{bat}}{W_\mathrm{take\text{-}off}} \end{aligned} \tag{10}$$

where $W_\mathrm{take\text{-}off}$ is the design (i.e. nominal maximum) take-off weight of the aircraft, and as such a convenient normalization term. It is possible to introduce the energy altitude associated to the energy storage systems as

$$h_\mathrm{e} = h_\mathrm{fuel} + h_\mathrm{bat}. \tag{11}$$

With the adoption of the energy altitude defined in Eq. 11, the optimality measure just introduced can be formalized analytically through the ratio $\frac{h_\mathrm{e}(t_f)}{h_\mathrm{e}(t_0)}$. By pursuing a higher value of this quantity, it is possible to find a solution that minimizes the energy expenditure over a flight. A convex cost function associated to this objective can be written as

$$J = \left(1 - \frac{h_\mathrm{e}\,(t_f)}{h_\mathrm{e}\,(t_0)}\right)^2, \tag{12}$$

which will take a null value when the final energy in the fuel and battery will be equal to the value at the beginning of the mission (ideal case), whereas it will be 1 if all energy sources are depleted at the end of the mission.

3.3. Optimization variables

In order to setup an optimization problem, it is necessary to formalize the identity of the optimization variables. As pointed out, the variables σ_{ICE}, σ_{EM} and P_{rec} are such to determine the power made available at every time instant. For a matter of convenience, it is possible to introduce the ratio

$$\tau_{\mathrm{rec}} = \frac{P_{\mathrm{rec}}}{\sigma_{\mathrm{ICE}} P_{\mathrm{ICE,n}}}, \tag{13}$$

which, similarly to σ_{ICE} and σ_{EM}, is limited between 0 and 1, representing the share of recharge power extracted from the current value of ICE power.

In order for the optimization problem to be numerically transcribed efficiently, yet in a sufficiently accurate fashion, it can be assumed that the profile of the mission be discretized in segments, corresponding to the phases of the flight. Considering for instance three segments, corresponding to climb, cruise and descent, the simplest mission profile coping with the requirements outlined in section 3.1 is readily assembled. For each segment, a single - constant - value of each power setting σ_{ICE} and σ_{EM} can be specified, and similarly a constant value of τ_{rec} can be assigned. This assumption yields a total of nine power setting variables for a reference mission profile with three legs.

As previously pointed out, the airspeed V is considered a degree of freedom, and similarly to the throttle parameters and recharge power ratio, it can be assigned for all three legs of a hypothetical flight profile. However, in the energy approach adopted for the balance equations introduced in the previous sections, a substantial difference exists when considering the phases of the flight where altitude is changing, i.e. climb and descent, and those where altitude is constant, i.e. cruise and loiter (even though the latter is not being considered in the current theoretical example). In analytic terms, while for describing flight segments where $\dot{h}$ is not null Eq. 4 is needed, Eq. 8 is sufficient when $\dot{h} = 0$. In the latter case, specific excess power, itself a function of speed, is completely translated into an acceleration, which in turn provides the speed evolution over time by integration. This implies that for constant-altitude segments the value of speed cannot be imposed as a function of time - that would result in an over-determined, ill-posed problem. Considering the example flight profile introduced here, while for climb and descent it is possible to specify a constant speed value and compute the resulting vertical speed for a given specific excess power, for cruise it is possible to assign only an initial value of the speed.

The optimization variables can be arranged into an array $\boldsymbol{q}$ as follows

$$\begin{aligned} \boldsymbol{q} = \big\{ & \sigma_{\mathrm{ICE}}^{\mathrm{climb}}, \sigma_{\mathrm{EM}}^{\mathrm{climb}}, \tau_{\mathrm{rec}}^{\mathrm{climb}}, V^{\mathrm{climb}}, \\ & \sigma_{\mathrm{ICE}}^{\mathrm{cruise}}, \sigma_{\mathrm{EM}}^{\mathrm{cruise}}, \tau_{\mathrm{rec}}^{\mathrm{cruise}}, V_{\mathrm{initial}}^{\mathrm{cruise}}, \\ & \sigma_{\mathrm{ICE}}^{\mathrm{descent}}, \sigma_{\mathrm{EM}}^{\mathrm{descent}}, \tau_{\mathrm{rec}}^{\mathrm{descent}}, V^{\mathrm{descent}} \big\}, \end{aligned} \tag{14}$$

where the identity of the speed variable for the cruise segment has been marked as $V_{\mathrm{initial}}^{\mathrm{cruise}}$ for the reasons just explained.

It should be noted that the adopted approach to describe airspeed does not guarantee continuity on the boundaries of each flight segment. By checking time histories (examples will be provided in the results section 4), it was noted that the instantaneous changes in airspeed are not very large on the boundaries between flight legs, further assuring that such inconsistency, happening only instantaneously, can be *de facto* neglected in terms of associated energy expenditure.

3.4. Evaluation of cost function and constraints

Provided the throttle settings, recharge power ratio and speed are assigned for the whole mission profile, the mission can be simulated carrying out a forward-in-time integration of Eq. 4, based on the current value of the power available and required, respectively computed from Eq. 1 and 5. The weight and energy of the battery and fuel can be updated in the process, based on Eq. 2 and 3. Similarly, the value of the air density ρ is updated as a function of current altitude h.

Figure 2 synthetically recalls the main functions in the forward-in-time integration process.

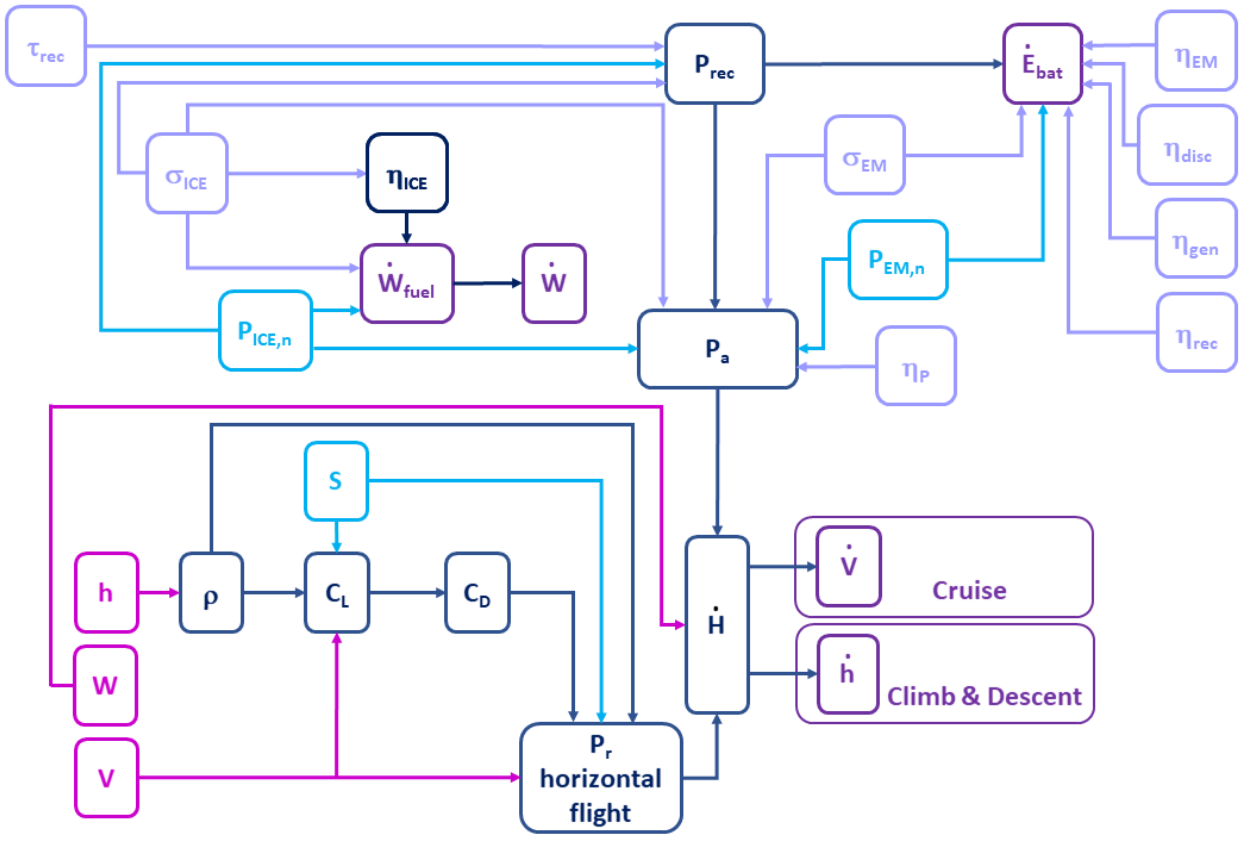

Figure 2: Functional scheme of a simulation step. Pink: current state. Light purple: assigned parameters (input) for the current time step. Light blue: constants. Dark blue: internal variables computed at current step. Dark purple: derivatives allowing forward-in-time integration.

As pointed out, for the climb and descent phases the starting and target altitudes are assigned, but as the airspeed V and specific excess power in Eq. 4 are given, the value of $\dot{h}$ is determined as a consequence.

The integration in time is carried out on a time domain featuring an extension which is not known *a priori*. Passing from the climb phase to cruise is subordinated to reaching the target altitude h_t, whereas passing from cruise to the descent phase happens upon reaching the target range R_t. It is clear that as a result of the adopted power settings and speed, i.e. for an assigned value of $\boldsymbol{q}$, a different trajectory will be obtained, as well as a different energy performance.

The values of all parameters in $\boldsymbol{q}$ are inherently bound between 0 and 1, whereas for speed parameters, bounds should be specified limiting the domain within acceptable physical limits. A lower bound for speed may be the stall value, computed on the actual take-off weight - i.e. not necessarily in the design weight condition - and clean aerodynamic configuration for safety (clearly, flapped conditions would provide higher lift coefficients and lower stall speeds), whereas for the top speed at a preliminary stage a physically meaningful arbitrary value may be specified corresponding to the aircraft category.

As the selection of the value of the optimization parameters will be demanded to the optimizer, the simulation may produce an outcome which is not necessarily physically acceptable. A proper set of constraints $\boldsymbol{S}(\boldsymbol{q})$ can be specified as follows to suitably steer the solution within physically viable boundaries.

The first two inequality constraints are related to the battery charging/discharging process. Batteries cannot be interested by a rate of change of the stored energy $\dot{E}_\mathrm{bat}$ exceeding the specific power of the battery, expressed by means of an assigned p_bat, which is inherent to the selected battery. As a result,

$$\begin{aligned} S_1 &: \max \dot{E}_\mathrm{bat} < \frac{p_\mathrm{bat} W_\mathrm{bat}}{g}, \\ S_2 &: \min \dot{E}_\mathrm{bat} > -\frac{p_\mathrm{bat} W_\mathrm{bat}}{g}. \end{aligned} \tag{15}$$

Further constraints related to the battery pertain to its energy level. The top value of the energy level should not exceed the technological limit bound to the energy density e_bat. Furthermore, nowadays batteries often feature a minimum state of charge ζ_min. The latter will be always above zero, and by keeping the battery at any time charged above that level, besides coping with technological limitations, will also prevent the charge to drop below zero, which would be non-physical. In analytic terms,

$$\begin{aligned} S_3 &: \max E_\mathrm{bat} < \frac{e_\mathrm{bat} W_\mathrm{bat}}{g}, \\ S_4 &: \min \frac{E_\mathrm{bat}}{E_\mathrm{bat,max}} > \zeta_{\mathrm{bat,\,min}}. \end{aligned} \tag{16}$$

A requirement which may be interesting to put on the solution is formally similar to S_4 in Eq. 16, yielding

$$S_5 : \frac{E_\mathrm{bat}(t_f)}{E_\mathrm{bat,max}} > \zeta_\mathrm{bat,final}, \tag{17}$$

where the value of the state of charge at the end of the flight - time t_f - is bound to be over a certain value $\zeta_{\text{bat,final}} > \zeta_{\text{min}}$. In consideration of the poor technical level of on-site services on smaller destination airports, it may be recommendable to keep a reserve of electrical energy for departure, as mentioned in section 3.1.

Finally, two requirements reflect the physics of the problem, and impose that the weight of the fuel and altitude be not below zero.

$$\begin{aligned} S_6 &: \min W_{\text{fuel}} > 0, \\ S_7 &: \min h > 0. \end{aligned} \tag{18}$$

3.5. Optimal problem

Based on the cost function defined in Eq. 12, the optimization parameters in Eq. 14 and the constraints described in Eq. 15 to 18, the optimal problem can be formalized as follows

$$\min_{\boldsymbol{q}} J \text{ s.t. } \boldsymbol{S}. \tag{19}$$

Figure 3 summarizes the scheme of the optimization process.

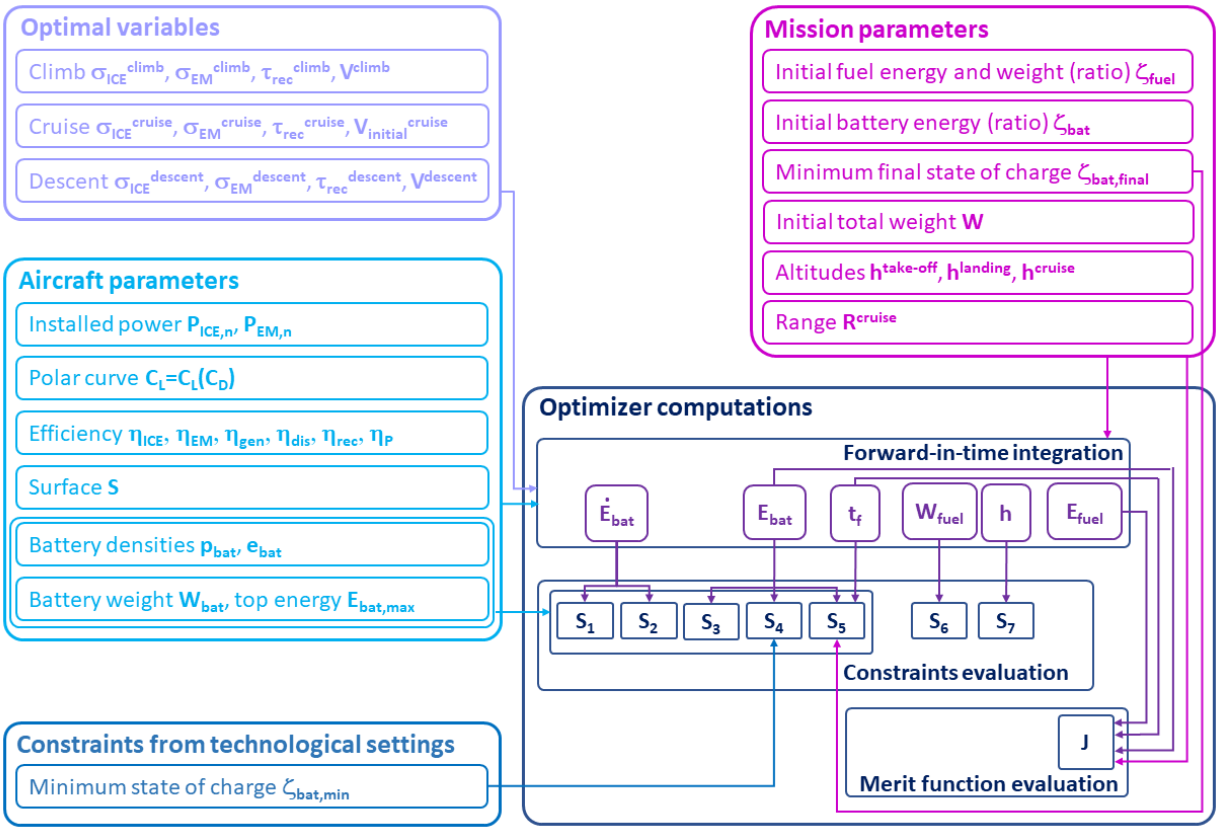

Figure 3: Scheme of the optimization process

As an observation concerning the choice of the cost function, it is clear that alternative functions to be optimized may be chosen, representing different objectives than the minimization of the expenditure of stored energy. In particular, it may be interesting to trade internal energy with kinematic/gravitational energy, as it is the case for speed rally aircraft or acrobatic aircraft - which promise to benefit significantly from hybrid-electric technology, also thanks to the extreme torque and acceleration characteristics of electric motors. In this sense, the adoption of an altitude quantity h_e, which is easily comparable to total altitude H often used to study the flight mechanics of high-performance aircraft, is not by chance, and paves the way to further optimal energy-based analysis which may be treated in future works, making use of the analytic framework presented herein.

In this work, we limit the scope of the analysis to the scenario outlined in sections 1 and 3.1, where it is interesting to carry out the optimization process to explore the performance of an aircraft in several off-design conditions. Considering the ensuing need to launch several optimization processes corresponding to different off-design conditions, care has been taken to keep the computational burden of the optimization low. Considering the set of optimization variables for each segment of the flight is already as high as 4, regardless of the type of leg in the sense described in section 3.3, the complexity of the flight profile has been kept limited to ease the obtainment of results, while simultaneously keeping their quality at a good level. Of course, adopting a more complete and in-depth description of the mission profile would be possible in proportion to the available computational resources.

4. Results

In this section the proposed methodology for the study of off-design performance seeking for an energy optimum will be illustrated on an example motor-glider. The design of this test-bed aircraft has been thoroughly illustrated in other works [8, 11, 12].

The aircraft is in the lower-weight sector of the general aviation category, which is where hybrid-electric power-trains are more likely to be industrially viable earlier [7], making the following results more interesting.

The scope of the analysis is two-fold. Firstly, it investigates performance results on a credible hybrid-electric aircraft concerning the recurring problem of a design flight profile flown with a fuel or electric energy provision which is not the design one. Secondarily, the results displayed herein treating this performance analysis problem illustrate the potential of the proposed optimal approach.

The outcome of the analysis, albeit clearly preliminary and not of general validity for other aircraft, shows an assessment of the performance which could be elaborated to bear a complement to the flight manual of a hybrid-electric aircraft, as it helps the pilot to choose the best settings for flying an intended mission, given the specific initial energy state on departure. Similarly, the maps produced in the results could represent the base components of a database to feed an automatic full-authority flight control computer, capable of automatically

selecting the optimal settings of the ICE and EM based on energy storage data read at departure, and on flight planning - i.e. on the actual mission requirements. Also in this sense, the results shown below are clearly still far from a complete database. Yet in the performance exploration phase to assess the potential of novel hybrid-electric propulsion concepts under investigation, these types of results allow to check what type of data could be obtained through the proposed off-design analysis approach, and bear some conclusions for a specific aircraft as well.

After quickly recalling the data of the aircraft used for the computations, extensive numerical results will be shown concerning the analysis of the energy-optimal mission performance obtained on a grid of changing departure energy conditions, both in terms of local (time histories) and general behavior (contour analysis). Further results will be presented trying to assess the effect of some specific parameters on the optimal solutions.

4.1. Aircraft data

The considered aircraft is a light, single-propeller, series-parallel hybrid-electric motor-glider. The basic data of the aircraft are recalled in Tab. 1 and 2.

$W_{\text{take-off}}$ [kgf]	585
$W_{\text{fuel,max}}$ [kgf]	42.6
W_{bat} [kgf]	38.2
$P_{\text{ICE,n}}$ [kW]	25.0
$P_{\text{EM,n}}$ [kW]	14.8
e_{bat} [Wh/kg]	136.5
p_{bat} [W/kg]	761.9
S [m^2]	9.6
$C_{\text{D,0}}^{\text{clean}}$	0.0110
K^{clean}	0.0128
$C_{\text{L,max}}^{\text{clean}}$	1.5

Table 1: Basic data for the example motor-glider.

It should be noted that only the clean polar has been reported and used in computations. This reflects the choice to neglect the terminal phases in the mission profile. Besides saving on computational time and reducing the complexity of the example as already pointed out, this choice is due to two reasons. Firstly, based on performed evaluations of the relative weight of each component of the mission profile, it has been realized that the relevance of terminal maneuvers is totally negligible compared to any other phase. Furthermore, from the viewpoint of an energy-optimal approach, especially take-off is usually an outlier, for due to safety

reasons reflected in the need to take-off in the shortest length possible, it is performed in normal practice close to or at full-power, and without draining mechanical power to recharge the batteries. In other words, the strict constraints typical to take-off, which completely define its energy performance *a priori*, would make treating this phase in an optimal way a computationally expensive and futile effort.

The power-train of the aircraft features a scheme well portrayed by Fig. 1, where part of the mechanical power produced by the ICE is conveyed towards the generator and through the electrical branch, whereas part goes directly to the gearbox feeding the propeller.

As pointed out in section 2.1, the model of the power-train accounts for a number of efficiency factors, which make it more realistic. The nominal values of these factors are reported in Tab. 2.

$\eta_{\mathrm{ICE,n}}$	0.30
η_{EM}	0.90
η_{gen}	0.90
η_{rec}	0.75
η_{dis}	0.75
η_{P}	0.80

Table 2: Efficiency data for the power-train of the example motor-glider.

For simplicity, all efficiency factors except η_{ICE} are kept constant to the nominal value, chosen to be representative of most regimes where the aircraft will be operating in flight. This assumption would have been excessively brutal for η_{ICE}, which is therefore considered as a function of the ICE thrust setting σ_{ICE}, yielding $\eta_{\mathrm{ICE}} = \eta_{\mathrm{ICE}}(\sigma_{\mathrm{ICE}})$. The dependency between the two parameters has been modeled based on a sine arc function [12], with the nominal value $\eta_{\mathrm{ICE,n}}$ considered as a maximum reached at $\sigma_{\mathrm{ICE}} = 1$, and the efficiency η_{ICE} dropping to a residual almost null value for σ_{ICE} approaching 0.

The basic design performance figures of the aircraft are reported in Tab. 3.

The values in Tab. 3 show the features of the mission considered in the design phase, and implicitly help to check what performance can be obtained with the considered aircraft.

4.2. Performance in off-design energy-optimal conditions

It is noteworthy that in the design phase take-off was correctly taken into account, with an impact on installed power. Also, the mission accounted for a loiter phase (Tab. 3). Both mentioned phases had to be performed at a non-zero altitude, as typical to a conservative design approach. A minimum final state of charge $\zeta_{\mathrm{bat,final}} = 0.15$ was specified for the batteries [12].

In the off-design analysis considered here, the mission requirements are changed as follows. As previously noted, the take-off phase, while demanding on power performance, is energetically negligible. The loiter

$L^{\text{take-off}}$ [m]	200
$h^{\text{take-off}}$ [m]	3000
V^{climb} [kn|m/s]	$1.2\text{V}_{\text{stall}}^{\text{landing}}$
$\dot{h}^{\text{climb}}$ [ft/min|m/s]	400|2.02
h^{cruise} [m]	3000
V^{cruise} [kn|m/s]	90|46.3
R^{cruise} [km]	300
h^{loiter} [m]	3000
V^{loiter} [m/s]	$0.9\text{V}^{\text{cruise}}$
T^{loiter} [min]	15
$\zeta_{\text{bat,final}}$	0.15
$V_{\text{stall}}^{\text{landing}}$ [kn|m/s]	40|20.6

Table 3: Performance for the design mission profile.

phase, required for modeling a holding pattern, is typically much reduced for smaller sport aircraft operating from local airfields with irrelevant congestion issues, and would add a complication and computational burden in spite of results of reduced practical interest if included in the present analysis as a parameter.

Following these considerations, three different set of mission requirements are considered. They share the general architecture of the mission profile, composed of three phases - climb, cruise and descent - as in the theoretical example suitably introduced in section 3.3. The features of the off-design mission profiles are presented in Tab. 4.

	Mission A	Mission B	Mission C
$h^{\text{take-off}}$ [m]	0	0	0
h^{cruise} [m]	3000	1000	3000
R^{cruise} [km]	300	450	300
h^{landing} [m]	0	0	0
$\zeta_{\text{bat,final}}$	0.8	0.8	0.1

Table 4: Mission performance data for the example motor-glider.

Mission A and C differ only for the requirements on final state of charge, which might be imposed to a higher value in view for instance of the absence of a recharging station on destination, in preparation for a return flight. Mission B trades cruise altitude with range of flight with respect to the requirements of reference mission A.

In order to better cope with real practice, due to the relatively low power-to-weight ratio of this motor-glider and the ensuing limited climb performance, the range requirement R^{cruise} in Tab. 4 is considered in the computation to be covered over both climb and cruise - i.e. the sum of the length of the trace of climb and cruise on the ground needs to be at least R^{cruise}. This too is not unusual in mission planning for light sport aircraft, especially if cruise altitude h^{cruise} is significantly high in consideration of an adopted aircraft category, as for the present case especially for mission A. Both take-off and landing are performed at sea level, implying that the aircraft in climb is ascending from sea level to h^{cruise}, and the contrary happens in descent.

4.2.1. Results for reference mission A

Considering the specifications defined as mission A on Tab. 4, the energy-optimal approach described in 3.4 and 3.5 is run on an 8-by-8 grid of energy-related initial conditions, characterized in analytic terms by values of ζ_{fuel} and ζ_{bat} changing between 0.4 and 1 every 0.1. The lower limit of the initial energy ratios has been chosen with a trial and error procedure, by preliminarily launching an analysis over a larger domain of initial conditions, and recording those conditions where the mission requirements could not be met - i.e. for which too low energy is loaded on board to cover the mission. Those conditions have been taken out of the analysis.

The adopted optimization algorithm is gradient-based. Experiments with different reasonable initial conditions show the robustness of the solutions, thus confirming the suitability of the considered numerical tool. No evident issues in the treatment of all constraints by the numerical algorithm have showed up.

Optimal throttle settings and recharge power. The results in terms of the optimal variables σ_{ICE}, σ_{EM} and τ_{rec} are shown in Fig. 4. From left to right are displayed the values assumed in climb, cruise and descent.

By quickly comparing the results for the climb phase (leftmost column) with those for the other two phases (other columns), it can be argued that this phase is the most critical for capturing an optimum for changing ζ_{fuel} and ζ_{bat}, as witnessed by the significant gradients in the solution map especially in terms of σ_{EM} and τ_{rec}.

More in depth, concerning $\sigma_{\text{ICE}}^{\text{climb}}$, in climb this is kept almost invariably very close to the maximum, i.e. close to $\sigma_{\text{ICE}}^{\text{climb}} = 1$. For lower values of the initial fuel weight ratio ζ_{fuel}, the use of the electric source, represented by $\sigma_{\text{EM}}^{\text{climb}}$, is decreasing for decreasing values of the initial electric charge ζ_{bat}, and tends rapidly to $\sigma_{\text{EM}}^{\text{climb}}$ almost null over a large area around the lower-left corner of the plot (i.e. for low ζ_{fuel} and ζ_{bat}).

Looking at the $\tau_{\text{rec}}^{\text{climb}}$ plot, again for lower ζ_{fuel}, the recharge ratio is very close or equal to zero. This shows that for lower values of ζ_{fuel}, and irrespective of the value of ζ_{bat}, all power from the ICE is dedicated in climb to aircraft propulsion. The electric motor contributes proportionately to the state of charge, with energy obtained only by draining the battery.

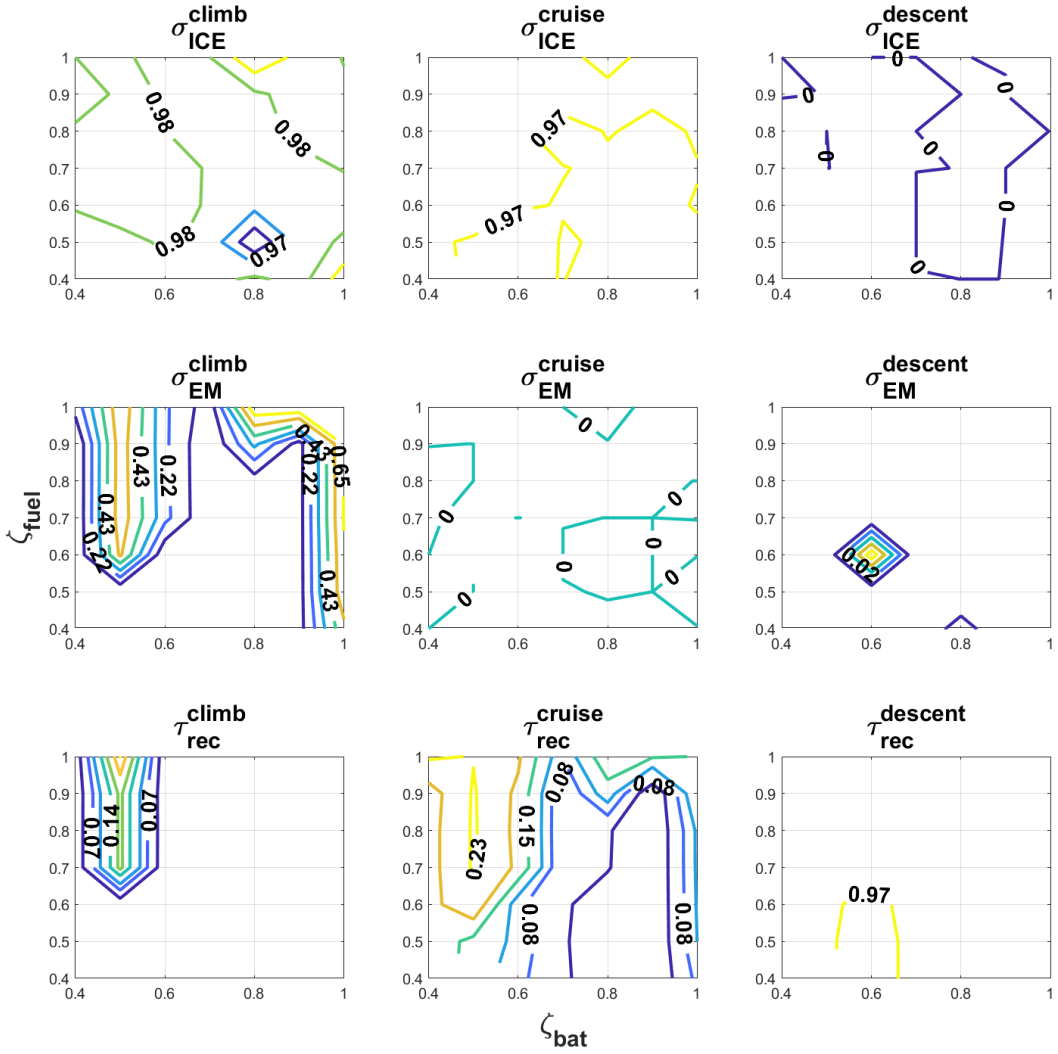

Figure 4: Optimal values of σ_{ICE}, σ_{EM} and τ_{rec} (from top to bottom) for different initial conditions ζ_{fuel} and ζ_{bat}. From left to right: values assumed in climb, cruise and descent. Mission A (Tab. 4).

Only for high values of fuel energy ζ_{fuel} and very low values of ζ_{bat} a recharge action is carried out in climb. Considering together the two plots for $\sigma_{\text{EM}}^{\text{climb}}$ and $\tau_{\text{rec}}^{\text{climb}}$, it is possible to notice that when there is a recharge action, the electric motor is also more significantly used, thus draining the battery, and causing battery depletion (as will be clear in the time histories below).

Concerning the cruise phase, similarly to the climb phase, the $\sigma_{\text{ICE}}^{\text{cruise}}$ value is generally close to the top value of 1, i.e. the ICE is kept running at almost full power. On the other hand, the EM is basically not used in this phase, as can be seen on the $\sigma_{\text{EM}}^{\text{cruise}}$ plot. Part of the ICE power is used to recharge the batteries, somewhat higher for low values of the ζ_{bat} and high ζ_{fuel}, which corresponds to a higher take-off weight and a lower initial battery charge. Coupled with the null EM power draining the batteries, this power flow produces a significant increase in battery energy.

From the rightmost plots in Fig. 4 it can be seen that the energy-optimal way to perform the descent phase is that of cutting the ICE and EM power down to a minimum close to 0. It can be argued that the requirement on the final battery charge $\zeta_{\text{bat,final}}$ expressed by constraint Eq. 17 is basically met already at the end of the cruise phase, therefore in descent no further charging is carried out. Consistently, the high value of the ratio $\tau_{\text{rec}}^{\text{descent}}$ is not associated to a significant $\dot{E}_{\text{bat}}$, for the ICE power flow this ratio is applied to is very low.

Optimal airspeed. The plots in Fig. 5 display the values of speed pertaining to the speed variables V^{climb}, $V_{\text{initial}}^{\text{cruise}}$ and V^{descent}.

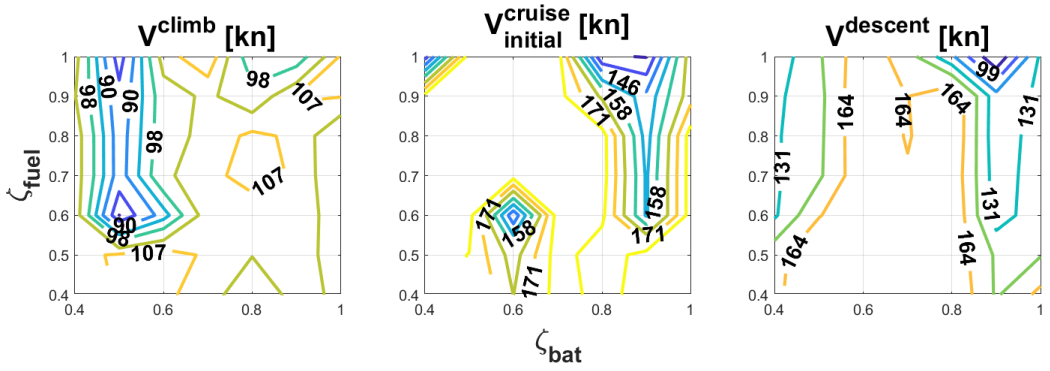

Figure 5: Optimal values of V^{climb}, $V_{\text{initial}}^{\text{cruise}}$ and V^{descent} for different initial conditions ζ_{fuel} and ζ_{bat}. Mission A (Tab. 4).

The leftmost plot, showing V^{climb}, highlights lower values of the climb airspeed for the same range of ζ_{fuel} and ζ_{bat} for which a recharge action is carried out. This suggests that for a lower initial battery charge ζ_{bat} and for higher aircraft weight - bound to higher ζ_{fuel} - a better global energy performance is obtained through a somewhat less aggressive climb, with the help of the EM and devoting part of the ICE power - always close to the top - to battery recharging.

Interestingly, the top values of optimal initial cruising speed $V_{\text{initial}}^{\text{cruise}}$ in the center plot of Fig. 5 are encountered in the same area where battery recharging is carried out (see $\tau_{\text{rec}}^{\text{cruise}}$ plot on Fig. 4). Furthermore, the airspeed values in cruise are generally much higher than the design values. Caution is required looking at this plot, which is not exactly representative of the actual airspeed assumed for the majority of the cruise, for the reason explained in section 3.3. However, considered together, these observations about cruise may show that an energy-optimal approach is such to reduce the time of flight as much as possible - by increasing speed - and even further if power is transferred to the batteries via the recharging process. This result may be typical to the aircraft considered here, featuring a good lift-to-drag ratio of a motor-glider for an extensive range of airspeed values in level flight, making flying at higher speeds energetically cheaper than usual.

The high speed encountered in the descent phase, associated to the close-to-null ICE and EM power as seen in Fig. 4 (rightmost plots), is in support of a tendency to increase energy performance by reducing the time extension of the mission as much as possible, and simultaneously preserve stored energy.

Spot analysis of trajectory, power components and energy quotas. Figure 6 displays a comparison of the time histories of altitude, distance traveled and airspeed for three couples $(\zeta_{\text{bat}}, \zeta_{\text{fuel}})$, i.e. three points on the map plot in Fig. 4 and 5. For the same three couples, the three plots in Fig. 7(a) show the time histories of available power P_{a}, required power for horizontal flight P_{r} and recharge power P_{rec}. Similarly, Fig. 7(b) show the energy quotas pertaining to stored fuel and battery energy. The selected couples share the same $\zeta_{\text{fuel}} = 0.7$, whereas the colors on Fig. 6 and 7 are blue solid for $\zeta_{\text{bat}} = 1.0$, red dashed for $\zeta_{\text{bat}} = 0.7$ and green dash-dotted for $\zeta_{\text{bat}} = 0.5$.

From Fig. 6, describing the flight trajectory and speed of the aircraft, it is possible to note that a marked difference exists in the climb performance for the intermediate considered $\zeta_{\text{bat}} = 0.7$ (red dashed curve) with respect to the other two. From the climb plots in Fig. 4, this choice of ζ_{bat} corresponds to a condition where no recharge is taking place, and an almost null EM power is used for flight. Correspondingly, from the P_{a} plot on Fig. 7, the power available is the lowest in this phase of the flight.

In terms of distance traveled (center plot on Fig. 6), the three solutions are very similar, showing little effect of pursuing an energy-optimal strategy coping with different ζ_{fuel} and ζ_{bat} on this parameter. Concerning speed (bottom plot on Fig. 6), it can be noticed how a similar initial speed in cruise for the different considered solutions is representative of a similar airspeed kept for the majority of the cruise, hence justifying the comments above concerning the $V_{\text{initial}}^{\text{cruise}}$ plot in Fig. 5. Yet caution is needed here, for the actual value of airspeed in cruise is significantly lower than the initial one.

Concerning the methodological comments presented in section 3.3, from Fig. 6 discontinuities in all time histories of airspeed can be spotted. These discontinuities are the result of the adopted flight mechanics modeling scheme, as explained previously (see Eq. 14). While on one side these steps in the time histories of airspeed are not physical, practice suggests that in presence of inertia phenomena, not accounted for in

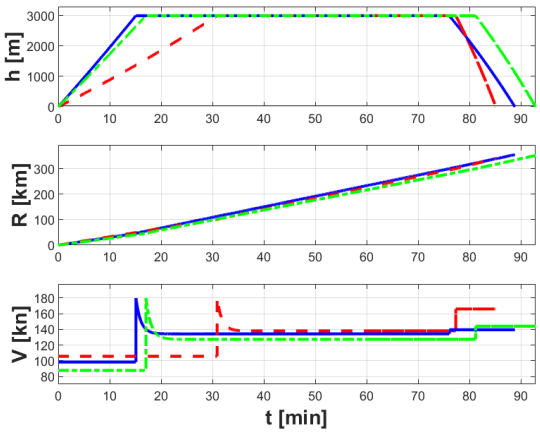

Figure 6: Time histories for energy-optimal solutions corresponding to $(\zeta_{\text{bat}}, \zeta_{\text{fuel}})$ of (1.0,0.7) in blue solid, (0.7,0.7) in red dashed and (0.5,0.7) in green dash-dotted. Top plot: altitude. Center plot: distance traveled. Bottom plot: airspeed. Mission A (Tab. 4).

the present work when joining together different legs of the flight, instead of a step, a less steep change of airspeed in time will take place in reality. Furthermore, considering all other plots in Fig. 6 and Fig. 7(b), it is apparent that no significant effect results from such airspeed steps, either on trajectory or energy components. In turn, this suggests that what will happen in reality, where inertia-related damping will be present, will be sufficiently similar to the prediction of the theoretical model adopted herein.

Looking at the three phases of the flight one by one, the values of airspeed are similar comparing the three considered cases.

From the power plots on Fig. 7(a), looking at the climb phase it is possible to notice how the higher power available P_{a} and a comparable power required P_{r} - bound to the selected speed, for the weight of the aircraft is the same for the three solutions, which feature the same ζ_{fuel} - is in agreement with the results on the airspeed and vertical speed - the former reported on the bottom plot of Fig. 6, the latter visible as a gradient in the initial phase of the flight on the top plot of the same figure.

In cruise, the power required evolves corresponding to a change in speed, to meet the power available. For the three selected conditions, it can be noticed that in the cruise phase there is always a recharge power, which is bound by definition to both $\tau_{\text{rec}}^{\text{cruise}}$ and $\sigma_{\text{ICE}}^{\text{cruise}}$. Especially for the case of lowest ζ_{bat} (green dash-dotted curve), the recharge power P_{rec} is relatively high, and recharge takes place both in climb and cruise.

The reason for that is not immediately apparent from the top plot in Fig. 7(b). It can be argued that in order to meet the requirements on final state of charge, the most disadvantageous initial condition (green dash-dotted line) is cured by a significant recharge power, which nonetheless in climb is associated to a depletion of the battery, implying an even higher recharging power in cruise. By comparison, the red-dashed

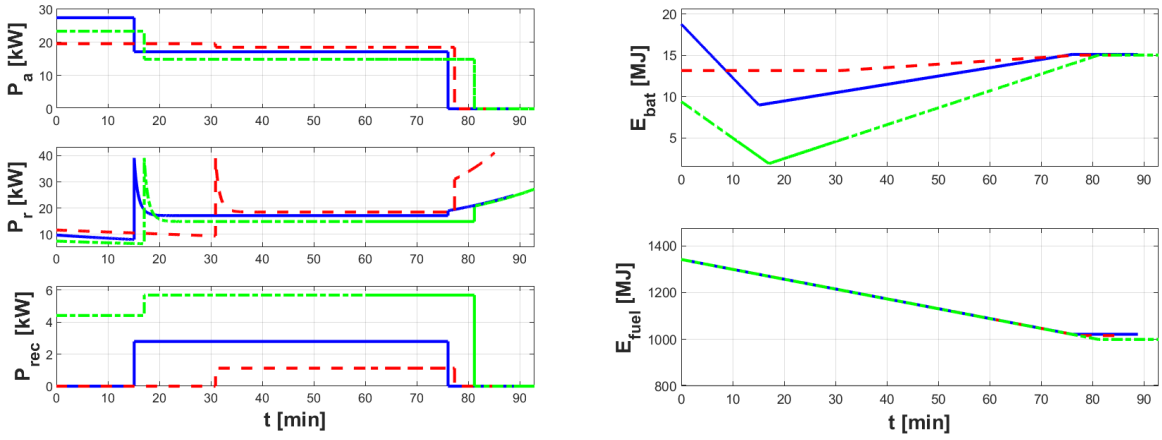

(a) (b)

Figure 7: Time histories for energy-optimal solutions corresponding to the same $(\zeta_{\text{bat}}, \zeta_{\text{fuel}})$ of Fig. 6. (a) power available, power required and recharge power. (b) battery energy and fuel energy. Mission A (Tab. 4).

curve, corresponding to an intermediate initial ζ_{bat}, shows how the state of charge is pulled up to the desired final value without any battery depletion. The reason for these differences is bound to the airspeed selected by the optimizer. This is generally lower for the lower considered ζ_{bat} values (green dash-dotted line), implying a lower required power, which in turn is met by a lower power made available by the ICE and EM, sparing fuel for the recharging process. Due to the lower speed, the mission lasts longer than for the other cases. This solution is qualitatively similar to that obtained for the top ζ_{bat} (blue solid curve), which is associated to intermediate speeds between those of the extreme ζ_{bat} cases (Fig. 6). The red dashed curve related to the intermediate ζ_{bat} case is associated to a higher speed in all phases, with an ensuing higher power required. This is met by a higher power made available by the ICE only for the cruise phase, resulting in a shorter mission. The values of J of the three solutions (not shown) are fairly similar, as can be argued from the energy plots on Fig. 7(b), but the strategies to obtain such results coping with the different initial energy conditions are somewhat different, as observed.

4.2.2. Effect of range and altitude requirements - mission B

Compared to mission A, the set of requirements defining the off-design mission B features an increased range and a decreased cruise altitude (see Tab. 4). Figure 8 and 9 report the behavior of the optimal variables for the same grid of ζ_{fuel} and ζ_{bat} considered in section 4.2.1.

Optimal throttle settings, recharge power and speed. Similarly to mission A, albeit much less extended in time due to the lower h^{cruise} requirement, climb appears as the most crucial phase in the seek for an energy optimum for changing ζ_{fuel} and ζ_{bat}, as can be noted through the presence of the most intense gradients in

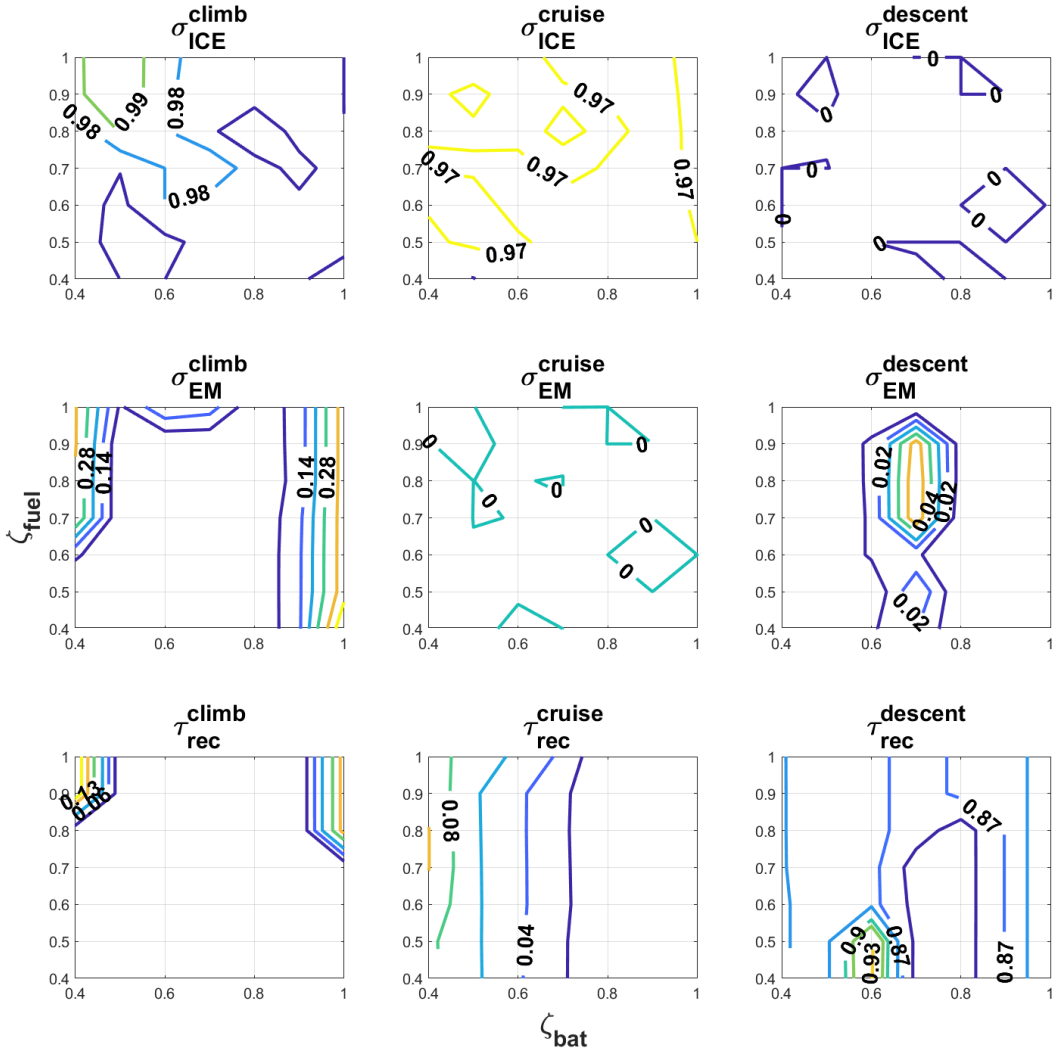

Figure 8: Optimal values of σ_{ICE}, σ_{EM} and τ_{rec} (from top to bottom) for different initial conditions ζ_{fuel} and ζ_{bat}. From left to right: values assumed in climb, cruise and descent. Mission B (Tab. 4).

the leftmost plots in Fig. 8. However, compared to the corresponding plots on Fig. 4, it appears that the EM is used less in mission B than in mission A also in climb, as witnessed by the generally lower values of $\sigma_{\mathrm{EM}}^{\mathrm{climb}}$. Similarly, the value of the $\tau_{\mathrm{rec}}^{\mathrm{climb}}$ appears very limited and close to 0 over the full considered domain in this phase. This shows that a reduced requirement in the climb phase, together with a requirement for a final state of charge $\zeta_{\mathrm{bat,final}} = 0.8$ (Tab. 4), can be met in a more energy-efficient way by simply limiting the use of the electric branch of the power-train (Fig. 1). Considering the fact that the mission is dominated by a very long cruise, where it can be seen the electric branch is not used ($\sigma_{\mathrm{EM}}^{\mathrm{cruise}}$ and $\tau_{\mathrm{rec}}^{\mathrm{cruise}}$ plots in Fig. 8), this behavior supports the concept that for flight profiles dominated by a cross-country phase the electric component of a hybrid-electric power-train is not a very relevant asset.

Interestingly, the electric component is used in climb for high values of fuel loaded, where the abundance of energy stored in fuel and the advantage of decreasing weight before the long cruising phase are effectively traded using some electric energy for climb performance (reflected in a high $\sigma_{\mathrm{EM}}^{\mathrm{climb}}$), and for very high ζ_{fuel}, also for recharging the batteries (higher $\tau_{\mathrm{rec}}^{\mathrm{climb}}$). Correspondingly, it should be noted that the climb airspeed is lower than in other larger areas of the map, where $\sigma_{\mathrm{EM}}^{\mathrm{cruise}}$ and $\tau_{\mathrm{rec}}^{\mathrm{cruise}}$ are roughly null (see left plot on Fig. 9). The drainage of ICE power for battery recharge, leading to a loss of power available, is compensated by the activation of the EM.

Similarly, for extremely low values of electric energy storage (lower ζ_{bat}) and higher weight (higher ζ_{fuel}), there is a need to recharge the batteries to reach the requirement on $\zeta_{\mathrm{bat,final}}$, and some electric power is used to support the climb, especially in view of the higher initial weight.

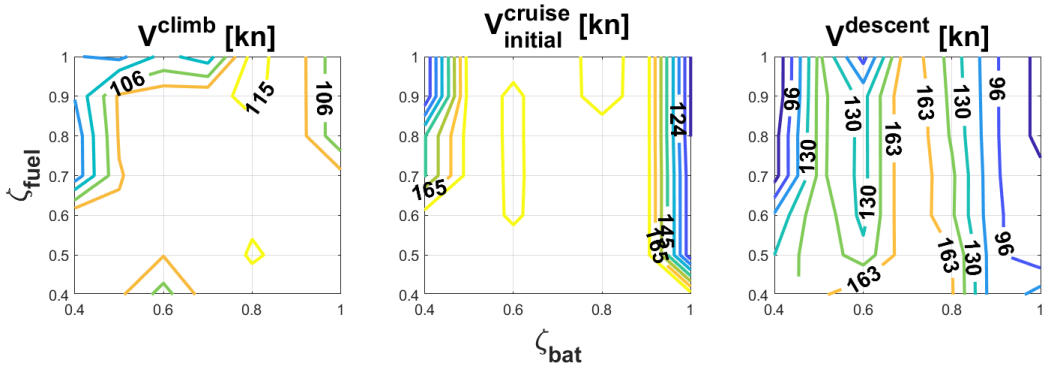

Figure 9: Optimal values of V^{climb}, $V_{\mathrm{initial}}^{\mathrm{cruise}}$ and V^{descent} for different initial conditions ζ_{fuel} and ζ_{bat}. Mission B (Tab. 4).

Comparing the center and right plots in Fig. 5 and 9, it can be noted that cruise is operated generally at lower speeds than for mission A, and significantly slower for $\zeta_{\mathrm{bat}} = 1$.

The need for a slower cruise in the $\zeta_{\mathrm{bat}} = 1$ condition can be explained with the chance to meet the final condition on $\zeta_{\mathrm{bat,final}}$ without reactivating the electric branch of the power-train after the end of the climb.

In other words, when the required $\zeta_{\mathrm{bat,final}}$ has been reached already at the end of the climb, flying somewhat slower for the rest of the mission profile, albeit for a little longer time, pays in terms of energy saved at the end of the flight. Of course, this result is better explained recalling that inefficiencies of the recharging process are thoroughly modeled here, thus transferring energy to the battery is an energetically expensive procedure. Furthermore, it should be observed that the good aerodynamic performance of the motor-glider wing, typically still well-performing also at lower airspeed, may be partly responsible for this result, making a standard ICE-propelled long cruise even more attractive.

Spot analysis of energy quotas. To appreciate this effect more, the plots of the time histories of E_{bat} and E_{fuel} are shown in Fig. 10. Here it is possible to reinstate what has been observed, in particular the different results in battery depletion in climb and the unneeded activation of the battery recharging process and of the EM - i.e. of the whole electric branch of the power-train - for the $\zeta_{\mathrm{fuel}} = 0.7$ case, corresponding to the blue solid line, for which the constraint on $\zeta_{\mathrm{bat,final}}$ is met before the cruising phase starts. It is also noteworthy that the difference on the fuel level at the end of the cruise phase for all three considered cases is really negligible, further testifying the marginal use of electric power needed in the flight, dominated by cruise - in other words, all three flight cases depend so deeply on fuel, that differences in fuel energy evolution are not noticeable, notwithstanding different recharging strategies.

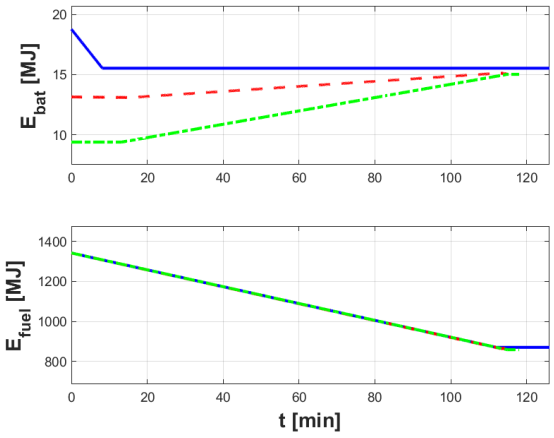

Figure 10: Time histories for energy-optimal solutions corresponding to $(\zeta_{\mathrm{bat}}, \zeta_{\mathrm{fuel}})$ of (1.0,0.7) in blue solid, (0.7,0.7) in red dashed and (0.5,0.7) in green dash-dotted. Battery energy and fuel energy. Mission B (Tab. 4).

Concerning descent, no significant difference with respect to the case of mission A can be reported from Fig. 8, 9 and 10, except a generally lower airspeed, which is compatible with the reduced cruise altitude - basically no energy storage is depleted in this phase.

4.2.3. Effect of final battery charge requirement - mission C

The final set of proposed mission requirements features a reduced $\zeta_{\text{bat,final}} = 0.2$, and flight mechanics parameters similar to mission A. The new set is reported in Tab. 4 as mission C. The plots in Fig. 11 and 12, compared to the respective plots in sections 4.2.1 and 4.2.2, allow to study the effect of this quantity.

Comparison of optimal results with other missions. A comparison with respect to Fig. 4 and 5 is especially interesting, due to the difference between the two scenarios A and C being the value of $\zeta_{\text{bat,final}}$, which tends to impose a greater battery recharging action in the former than in the latter.

As a consequence of that, it can be noticed on the $\tau_{\text{rec}}^{\text{climb}}$ plot in Fig. 11 how the recharge action is limited to a very small area of the analyzed domain of (ζ_{bat},ζ_{fuel}), and even there, associated to smaller $\tau_{\text{rec}}^{\text{climb}}$ intensities.

On the other hand, interestingly the EM is activated for almost all considered initial energy conditions in climb, differently from the mission A (and B) case ($\sigma_{\text{EM}}^{\text{climb}}$ plot on Fig. 11). This tends to support that the EM is energetically convenient in case no battery recharging process is needed to sustain its use. As the requirement on final stored energy is low for mission C, climb can be profitably sustained by the EM without depleting the batteries below $\zeta_{\text{bat,final}}$.

The airspeed in climb tends to be slightly higher than for mission A (compare left plot on Fig. 5 and 12), and considering mission C, a good match can be observed for a large number of initial energy conditions between the higher speeds and the higher throttle setting $\sigma_{\text{EM}}^{\text{climb}}$ of the EM. This is in accordance with the use of both the EM and ICE to sustain only flight performance.

Concerning cruise and descent, for almost all initial energy conditions the σ_{ICE}, σ_{EM} and τ_{rec} optimal solutions are largely similar, showing a high use of the ICE, and little use of the EM and battery recharging capability of the power-train (see plots on the center and right columns of Fig. 11). Similarly to what happens for climb, the values of speed are slightly higher than in mission A case (center and right plots on Fig. 12).

Spot analysis of trajectory and energy quotas. The time histories of altitude, distance traveled and airspeed are shown in Fig. 13, for the same selection of initial conditions considered in Fig. 6 and 7. Similarly, in Fig. 14 the time histories of battery energy and fuel energy are shown. From the time histories in Fig. 13, it can be observed that the three solutions, albeit all optimal and even associated to very similar values of J (not shown), bear some dissimilarities, especially comparing the one associated to $\zeta_{\text{bat}} = 0.7$ (red dashed line) to the other two. This is true especially in descent, where a very reduced airspeed is associated to a prolonged mission. This result might be the effect of a reduced gradient of the merit function with respect to this variable, as the descent phase in this mission is not associated to any power (null $\sigma_{\text{ICE}}^{\text{descent}}$ and $\sigma_{\text{EM}}^{\text{descent}}$), implying no use of stored energy, which is what the adopted J considers, as per Eq. 12. From the same Fig. 13 it can be noted how the cruise speed kept for the majority of the cruise is visually identical for the three considered solutions, in agreement with the use of the same power settings, and with a similar weight

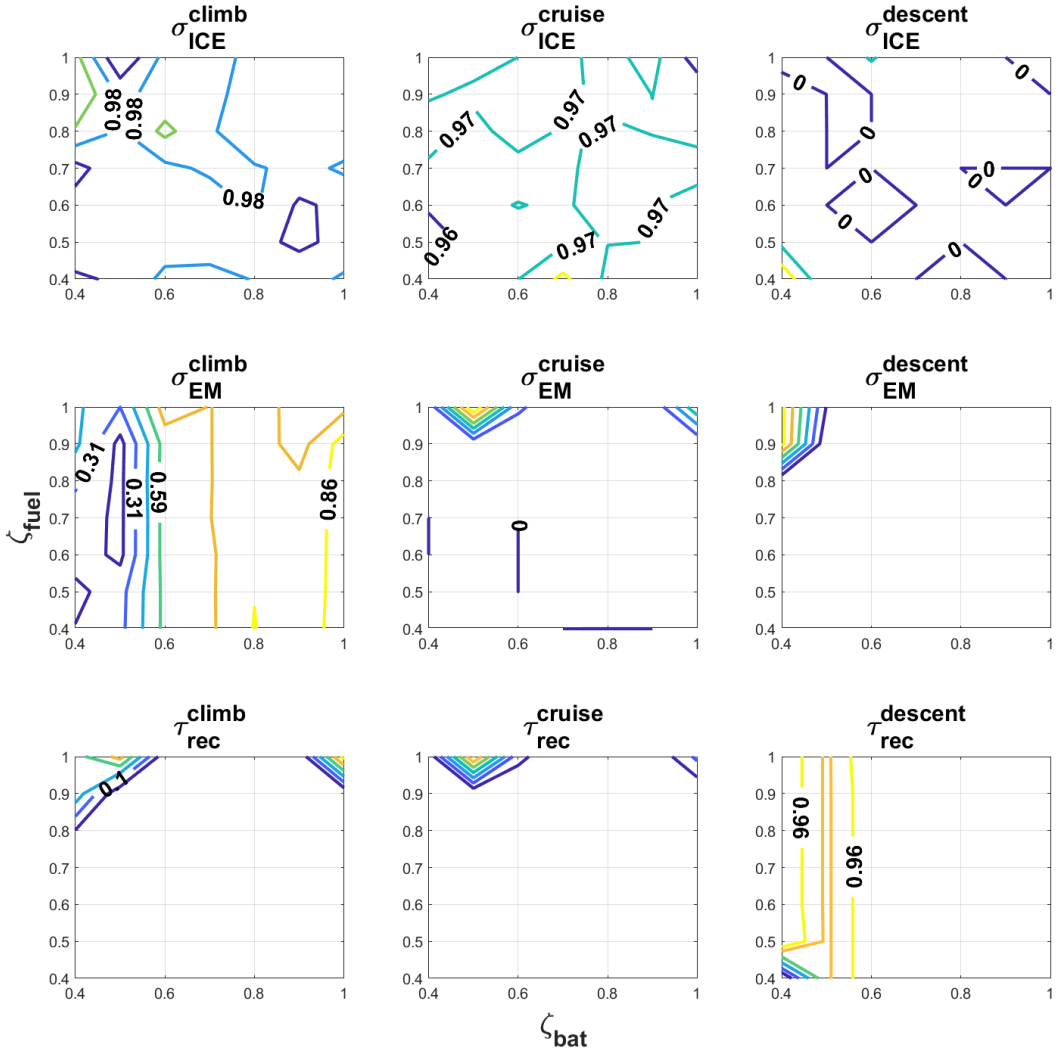

Figure 11: Optimal values of σ_{ICE}, σ_{EM} and τ_{rec} (from top to bottom) for different initial conditions ζ_{fuel} and ζ_{bat}. From left to right: values assumed in climb, cruise and descent. Mission C (Tab. 4).

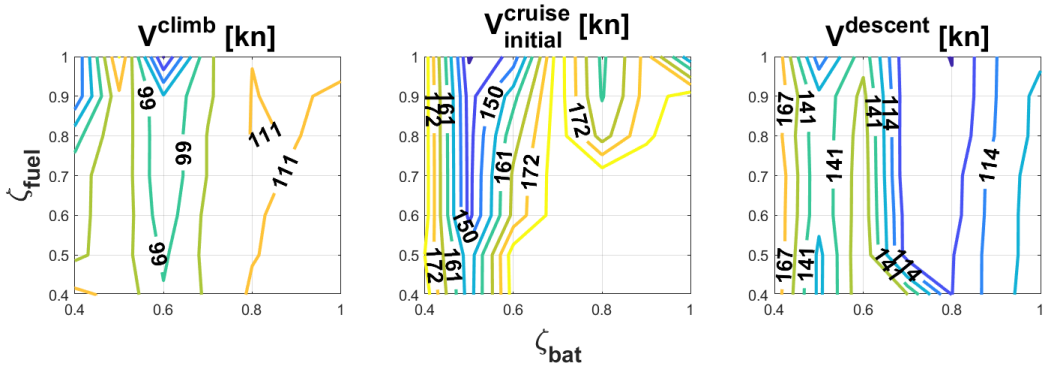

Figure 12: Optimal values of V^{climb}, $V^{\text{cruise}}_{\text{initial}}$ and V^{descent} for different initial conditions ζ_{fuel} and ζ_{bat}. Mission C (Tab. 4).

at the beginning of the cruise. The latter equality in weight at the beginning of the cruise phase is obtained notwithstanding rather different climb profiles, especially considering the curve associated to $\zeta_{\text{bat}} = 0.5$ (green dash-dotted) with respect to the other two. However, this effect is not strange considering the initial weight at the beginning of the flight in the three considered cases is the same - same ζ_{fuel} - and no recharging takes place.

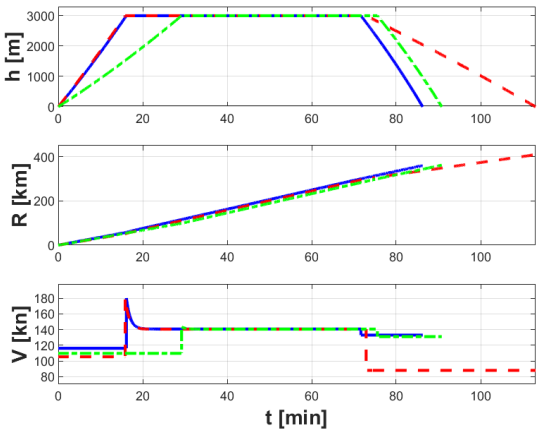

Figure 13: Time histories for energy-optimal solutions corresponding to $(\zeta_{\text{bat}}, \zeta_{\text{fuel}})$ of (1.0,0.7) in blue solid, (0.7,0.7) in red dashed and (0.5,0.7) in green dash-dotted. Top plot: altitude. Center plot: distance traveled. Bottom plot: airspeed. Mission C (Tab. 4).

Considering descent, looking at the energy time histories in Fig. 14, it can be seen that the solutions are different in terms of final battery energy, and albeit less visibly for a scale effect, also in terms of final fuel energy. In particular, the final battery energy for the red-dashed curve associated to $\zeta_{\text{bat}} = 0.7$ is significantly lower than the green dash-dotted one, associated to $\zeta_{\text{bat}} = 0.5$, whereas their respective positions are swapped considering E_{fuel} at final time. Interestingly, the value of fuel energy is fairly similar at the beginning of the

descent phase, but the battery charge value is higher for the green dash-dotted line. This can be possibly interpreted considering that the greater speed in descent for the case corresponding to the green dash-dotted line is associated to more ICE power and a lower time for the mission, whereas the red-dashed line features a dual behavior, sparing more fuel in view of the lower available battery energy at the beginning of the descent.

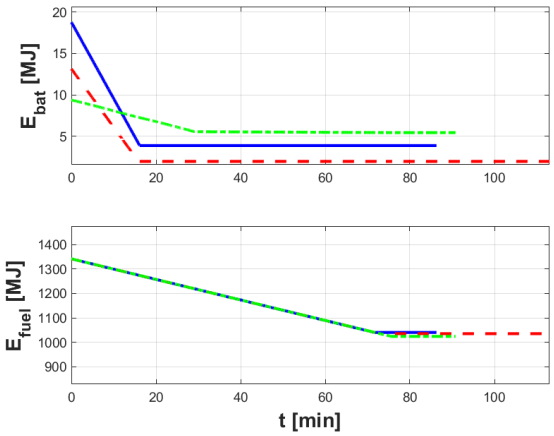

Figure 14: Time histories for energy-optimal solutions corresponding to the same $(\zeta_{\text{bat}}, \zeta_{\text{fuel}})$ of Fig. 13. Battery energy and fuel energy. Mission C (Tab. 4).

As said above, the overall stored energy level at the end of the mission - measured through J - is not strongly dissimilar, showing similarly to climb a virtually equal - albeit complicated - trade-off between ICE power setting, speed and time, reflecting in a trade-off between the final values of E_{bat} and E_{fuel}.

5. Conclusions and outlook

To the aim of analyzing the off-design performance of an assigned hybrid-electric aircraft, the present paper has introduced first a suitable model of a hybrid-electric power-train. Subsequently, that model has been interfaced with an energy-based description of an aircraft in flight, capable of rigorously accounting for those phases of the flight most impacting on energy performance.

In configuring the off-design analysis, it was noted how the latter can be treated as an optimal design problem, where most features of the aircraft are assigned, but the power settings of both the fuel-burning and electric part, together with the battery recharge power and the airspeed to keep in the different legs of the flight, constitute the variables of an optimal computation. This computation may be set up to target different goals, one among them being the energy expenditure over an assigned flight profile. In order to mathematically set up the corresponding optimal problem, suitable energy altitudes pertaining to the two available sources of energy (fuel and batteries) have been defined.

The methodology has been illustrated at a theoretical level based on a generic series-parallel power-train, yet featuring a single internal combustion engine and a single electrical motor. While this can be seen as a limitation, it can be noted that no major functional areas in the power-train model are overlooked, whereas for a multi-power-plant aircraft the proposed scheme of the power-train may feature basically the same components in larger numbers. From the viewpoint of the presented optimization, this would imply a greater complexity and more optimization parameters - with an ensuing increase in computational burden -, but without any major theoretical implications.

In the same fashion, the mission considered for the theoretical setup of the optimization, as well as in the results, is of course simple and hypothetical, but it is well representative of a cross-country mission for lighter sport aircraft, which are those for which the adopted scheme of a simple power-train is most suited, and also represent the category where hybrid-electric power-trains are most likely to be adopted first in the near future.

In the results section, centered on a particular aircraft test-bed considered in previous works on the topic in order to help comparisons and speculations, a thorough comparative analysis of the features and behavior of the energy-optimal solutions for three off-design target missions has been proposed, and considering several combinations of initial energy conditions. This off-design scenario has been investigated due to its practical relevance, bound to the lack of fuel refilling and battery recharging stations on airfields interested by light aviation aircraft activities. The results of the analysis tend to exhibit a good regularity and physical acceptability both in terms of maps for changing initial conditions and of time histories of spot-selected solutions.

Considering the specific case of the motor-glider adopted herein as a test-bed and the off-design missions analyzed, it has been noted that much power from the electric motor is used in climb. Correspondingly, especially when the requirement on final battery charge is stringent, the combustion engine is used to recharge the batteries, drained by the intense use of the electrical motor. Recharging takes place especially in cruise, where the electrical motor is barely used. When the requirement on climb is milder - i.e. the aircraft needs to climb to a lower cruising altitude - in conjunction with a stringent requirement on the final state of charge of the battery, the electrical component of the power-train tends to be used less also in climb. On the other hand, when the requirement on the final state of charge is made less stringent, the electrical motor is used especially in climb, but without correspondingly recharging the battery. It may be argued that the use of the electrical motor is more energetically optimal when less or no recharging is needed. This tends to support that battery recharging process is the most energy-critical in a hybrid-electric power-train.

Looking at the sometimes complex trade-off and intricate relationships between the components of the array of the optimal parameters and trying to establish a correlation with the outcome of the optimization runs, the advantage of a holistic approach, capable of considering several characteristics of the aircraft and

mission together, in order to automatically yield an accurate energy-optimal power-management strategy, is clearly apparent. This tends to support the validity of the presented optimal approach to power-management as a general-purpose tool, as it first and foremost tackles the power-management strategy design problem producing physically meaningful results in an efficient way, without brutal approximations on the physical model of the aircraft in flight. This feature of the approach in turn allows to profitably deploy it to map the off-design characteristics of an aircraft with relatively little effort, as shown in the results.

In order to make this solution more technologically applicable, the chance to adopt a table look-up approach - where results from optimization runs in several scenarios are used to create a database of optimal solutions for a number of diverse off-design conditions - instead of an online optimization, carried out on an on-board computer based on the actual planned mission and initial state, has to be considered to save on computer power and cost and to increase reliability, in face of a decrease in the accuracy of the optimal solution. The trade-off between these technical solutions has to be assessed. Testing the optimal solutions on more complex simulators, accounting in particular for disturbances to the planned mission as given by not predicted wind and faults or inaccuracies in the measurements systems, will likely constitute the next step of this research.

Acknowledgements

The contribution of Prof. Stefano Cacciola of the Department of Aerospace Science and Technology, Politecnico di Milano, in the discussion and revision of this paper is gratefully acknowledged.

Declaration of conflicting interests

The Author declares that there is no conflict of interest.

Funding

This research received no specific grant from any funding agency in the public, commercial, or not-for-profit sectors.

References

[1] C.A. Hall, and D. Crichton, Engine and Installation Configurations for a Silent Aircraft, ISABE, 1164(2005) 1-12.

[2] R. Kawai, Quiet Cruise Efficient Short Take-Off and Landing Subsonic Transport System, Technical Report NASA/CR2008-215141, NASA Glenn Research Center, Cleveland, OH, 2008.

[3] D. Miljkovic, J. Ivoevic, and T. Bucak, Psycho-Acoustical Ergonomics in a Light Aircraft Interior, in: 5th International Ergonomics Conference, Zadar, Croatia, June 12-15, 2013.

[4] G.E. Bona, M. Bucari, A. Castagnoli, and L. Trainelli, Flybrid: Envisaging the Future Hybrid-Powered Regional Aviation, in: AIAA/3AF Aircraft Noise and Emissions Reduction Symposium, Atlanta, GA, June 16-20, 2014.

[5] M.K. Bradley, and C.K. Droney, Subsonic Ultra Green Aircraft Research: Phase 2. Volume 2; Hybrid Electric Design Exploration, Technical Report NASA/CR-2015-218704/VOL2, NASA Langley Research Center, Hampton, VA, 2015.

[6] F. Bigoni, A. Moreno-Perez, F. Salucci, C.E.D. Riboldi, L. Trainelli, Design of Airport Infrastructures in Support of the Transition to a Hybrid-Electric Fleet, in: Advanced Aircraft Efficiency in a Global Air Transport System Conference (AEGATS 2018), Toulouse, France, October 23-25, 2018.

[7] *MAHEPA* - Modular Approach to Hybrid-Electric Propulsion Architecture, mahepa.eu, EU-Funded H2020 Project, Grant N.723368, 2016.

[8] C.E.D. Riboldi, and F. Gualdoni, An Integrated Approach to the Preliminary Weight Sizing of Small Electric Aircraft, Aerospace Science and Technology, 58(2016) 134-149.

[9] C. Friedrich, and P.A. Robertson, Hybrid-Electric Propulsion for Aircraft, Journal of Aircraft, 52(2015) 176-189.

[10] B.J. Brelje, and J.R.R.A. Martins, Electric, Hybrid, and Turboelectric Fixed-Wing Aircraft: A Review of Concepts, Models, and Design Approaches, Progress in Aerospace Sciences, 104(2019) 1-19.

[11] C.E.D. Riboldi, F. Gualdoni, and L. Trainelli, Preliminary Weight Sizing of Light Pure-Electric and Hybrid-Electric Aircraft, Transportation Research Procedia, 29(2018) 376-389.

[12] C.E.D. Riboldi, An Optimal Approach to the Preliminary Design of Small Hybrid-Electric Aircraft, Aerospace Science and Technology, 81(2018) 14-31.

[13] G. Paganelli, T.M. Guerra, S. Delprat, J.-J. Santin, M. Delhom, and E. Combes, Simulation and Assessment of Power Control Strategies for a Parallel Hybrid Car, Proceedings of the Institution of Mechanical Engineers, Part D: Journal of Automobile Engineering, 214(2000) 705-717.

[14] C. Musardo, G. Rizzoni, Y. Guezennec, and B. Staccia, A-ECMS: An Adaptive Algorithm for Hybrid Electric Vehicle Energy Management, European Journal of Control, 11(2005) 509-524.

[15] Y. Xie, A. Savvaris, A. Tsourdos, J. Laycock, and A. Farmer, Modelling and Control of a Hybrid Electric Propulsion System for Unmanned Aerial Vehicles, in: Proceedings of the 2018 IEEE Aerospace Conference, Big Sky, MT, March 3-10, 2018.

[16] C. Pornet, and A.T. Isikveren, Conceptual Design of Hybrid-Electric Transport Aircraft, Progress in Aerospace Sciences, 79(2015) 114-135.

[17] D.P. Raymer, Aircraft Design: A Conceptual Approach, AIAA Education Series, Fifth Edition, 2012.